Dithering-amplitude dependence of STM-regulated dynamic lateral force microscopy maps on Si(111)7×7

Naruo Sasaki,[1,*] Shigeki Kawai,[2,3] and Hideki Kawakatsu[2]

[1]*Department of Materials and Life Science, Faculty of Science and Technology, Seikei University, 3-3-1 Kichijoji-Kitamachi, Musashino-shi, Tokyo 180-8633, Japan*

[2]*Institute of Industrial Science, The University of Tokyo and CREST, Japan Science and Technology Agency, 4-6-1 Komaba, Meguro-ku, Tokyo 153-8505, Japan*

[3]*Department of Physics, University of Basel, Klingelbergstrasse 82, 4056 Basel, Switzerland*

(Received 20 September 2009; revised manuscript received 13 October 2009; published 3 November 2009)

Model simulation of dynamic lateral force microscopy (DLFM) regulated by scanning tunneling microscopy (STM) has been performed. The simulated STM/DLFM maps on Si(111)7×7 exhibit marked transitions depending on the lateral dithering amplitude, and they can successfully reproduce the experimentally acquired maps for a wide range of operating conditions. This work describes the direct calibration of dithering-amplitude-induced artifacts of STM/DLFM maps on Si(111)7×7 for a small time-averaged tunneling current corresponding to a tip-sample distance larger than 5 Å, where the atomic relaxation of the tip and the sample is sufficiently small.

DOI: 10.1103/PhysRevB.80.193402 PACS number(s): 68.37.Ps, 34.20.Cf, 68.37.Ef, 68.35.Af

Measurement techniques for lateral forces on the order of magnitude of piconewtons are important for controlling the atomic-scale ultralow friction[1] and superlubricity.[2] Dynamic force microscopy has been used both directly and indirectly as a reproducible and nondestructive method for detecting the lateral force. Dynamic vertical atomic force microscopy[3] indirectly detects the lateral interactions. First, a two-dimensional (2D) interaction potential map is extracted via a measured frequency shift map along the vertical direction.[4] Then, the lateral force and force gradient are calculated by differentiating V as $F_i=-dV/dx_i$ and $F_i'=dF_i/dx_i$, ($x_i=x$ or y). Although this method is not an *in situ* measurement, it can successfully obtain the lateral atomic resolution with high accuracy.[5–9]

On the other hand, dynamic lateral force microscopy (DLFM) can directly observe the frequency shift Δf_{TR} and energy dissipation.[10–12] In this method, the unavoidable thermal drift of the tip-sample distance at room temperature (RT) is excluded by controlling the tip-sample distance using a constant time-averaged tunneling current $\bar{I}_t$. In our previous work,[13] the simulated and experimental maps were compared. Both the simulated and experimental scanning tunneling microscopy (STM) profiles and DLFM maps for $\bar{I}_t=0.6$ nA and $A_{\mathrm{dith}}=0.81$ Å are in good agreement. Here, the lateral dithering amplitude A_{dith} must be set on the order of magnitude of sub-Angstroms. Furthermore, A_{dith} dependence of the two-dimensional pattern of STM-regulated DLFM (STM/DLFM) maps is also revealed. Therefore, in the present work, thoroughgoing studies of the effect of A_{dith} on STM/DLFM have been performed theoretically and experimentally. The direct calibration of A_{dith}-induced artifacts observed in STM/DLFM maps becomes possible under the condition that the tip is located far away from the sample surface, in which case the atomic relaxation of the tip and sample can be neglected.

The simulation method of STM/DLFM is shown in Fig. 1(a). The input parameters are the time-averaged tunneling current of STM, I_0, and the lateral dithering amplitude of the cantilever, A_{dith}. For each raster scanning position (x,y), the equation $\bar{I}_t(x,y,z;A_{\mathrm{dith}})=I_0$ is numerically solved to obtain the STM profile, $z_{\mathrm{STM}}(x,y)\equiv z(x,y;A_{\mathrm{dith}},I_0)$. Here, the time-averaged tunneling current is calculated as follows:

$$\bar{I}_t(x,y,z;A_{\mathrm{dith}})=\frac{1}{2\pi}\int_0^{2\pi} I_t(x_{\mathrm{TR}}+A_{\mathrm{dith}}\cos\theta)d\theta, \qquad (1)$$

where x_{TR} denotes the lateral dithering coordinate of the tip. Above the obtained STM profile, $z_{\mathrm{STM}}(x,y)$, the frequency shift along x_{TR}

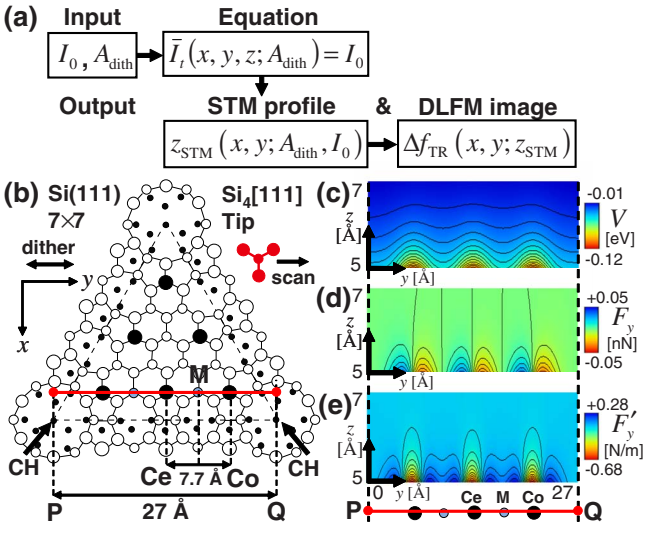

FIG. 1. (Color online) (a) Algorithm of the simulation method for STM/DLFM. (b) Schematic illustration of the rigid model: half part of the Si(111)7×7 surface and the Si_4[111] tip. (c) y-z maps of the total energy V, (d) lateral force F_y, and (e) lateral force gradient F_y' along P-Q. The approximately vertical lines in (d) indicate the positions corresponding to $F_y=0$.

$$\Delta f_{\mathrm{TR}}(x,y;z_{\mathrm{STM}}) = -\frac{f_{\mathrm{TR}}}{2\pi k_{\mathrm{TR}} A_{\mathrm{dith}}} \int_0^{2\pi} F_{\mathrm{TR}}(x_{\mathrm{TR}} + A_{\mathrm{dith}} \cos\theta)\cos\theta d\theta, \quad (2)$$

is calculated to obtain the DLFM image,[14,15] where k_{TR}, f_{TR}, and F_{TR} denote the effective torsional spring constant, torsional resonant frequency of the cantilever, and short-range tip-surface interaction force along the tip-dithering direction, respectively.

The tunneling current I_t and the lateral force $F_i(i=x,y)$ can be calculated using any type of *ab initio* or empirical method. First, I_t is calculated by the independent-orbital approximation,[11,16] where the conductance distributions derived from the overlaps of the p_z components between the tip and surface atoms are summed up as $I_t = \Sigma_j I_t^j$; $I_t^j \propto \cos^4\theta e^{-2\kappa r}$. Here, j denotes the index of all the adatoms, rest atoms, and corner holes of the surface, whose coordinates were obtained by Brommer *et al.*[17] using the first-principles simulation and are assumed to be rigid. r and θ denote the distance between the single tip-apex atom and the surface atoms and the angle between the tip-surface bond and the z axis, respectively. A typical decay constant of $\kappa = 0.96$ Å^{-1} (Ref. 16) is adopted. The tip-sample distance z is defined as the vertical distance between the rigid tip-apex atom and the rigid center (Ce) adatom. Here, the long-range van der Waals and electrostatic interaction forces are independent of the atomic site, although they homogeneously increase in magnitude as the tip approaches the sample. Therefore, the long-range interactions do not affect the STM/DLFM measurement if the tip dithering is controlled perfectly parallel to the sample surface. Thus, only the short-range Si-Si covalent lateral force F_y is considered. F_y [Fig. 1(d)] and F_y' [Fig. 1(e)] along P-Q are calculated by differentiating the total energy V [Fig. 1(c)] that was obtained by fitting the sum of the empirical Morse-potential functions between the Si$_4$[111] tip and the Si(111)7×7 surface[15] to the first-principles simulated results between the Si tip and the Si(111) surface.[18] Figure 1(d) shows, $F_y \simeq 0$ at Ce, corner (Co) adatom, and the middle (M) position between the neighboring Ce and Co for 5 Å$\leq z \leq$7 Å. It is noted that the rigid single-atom tip and the rigid Si$_4$[111] tip are used for calculating I_t and F_y, respectively. The latter tip is made by adding three atoms to the apex atom along the (111) direction.

As shown in Figs. 2 and 3, the A_{dith} dependence of the STM/DLFM maps for $\bar{I}_t$=0.5 nA is simulated for 0.37 Å $\leq A_{\mathrm{dith}} \leq$7.6 Å$\simeq L$. L=7.7 Å corresponds to the nearest-neighbor distance between Ce and Co along the y-dithering direction. The transition of the two-dimensional pattern reproduces the experiment extremely well. Here, the experiment was performed using a homemade ultrahigh vacuum DFM operating at RT.[13,19–21] The torsional resonance mode of a commercially available Si cantilever (Nanosensor NCH-SSS) was used to detect the tip-surface interaction. The tip and sample preparations have been described in previous works.[13,19] The experimental parameters f_{TR}=2.2 MHz and k_{TR}=1250 N/m were used in the simulation.

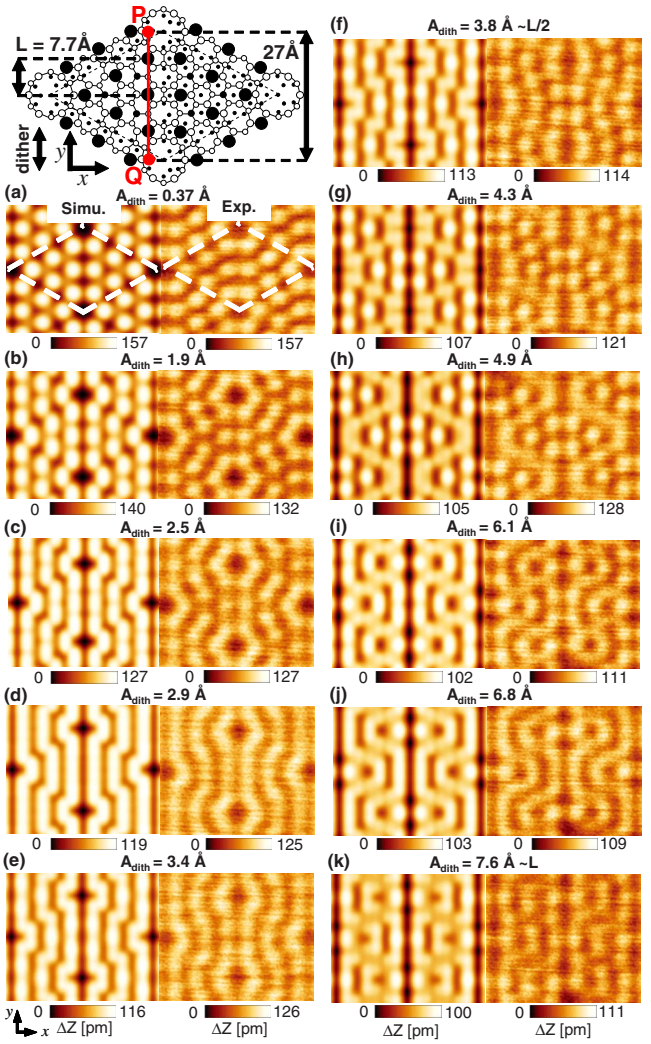

FIG. 2. (Color online) (a) Simulated (left) and experimental (right) STM topographies for A_{dith}= (a) .37, (b) 1.9, (c) 2.5, (d) 2.9, (e) 3.4, (f) 3.8($\simeq L/2$), (g) 4.3, (h) 4.9, (i) 6.1, (j) 6.8, and (k) 7.6($\simeq L$) Å. Imaging parameters: $\bar{I}_t$=0.5 nA and V_{bias}=1.8 V.

The simulated and experimental STM profiles exhibit quite similar transitions along P-Q with an increase in A_{dith} as follows: bright spots at Ce and Co [Fig. 2(a)] → enlarged bright spots and stripe [Figs. 2(b)–2(d)] → bright spots at M [Figs. 2(e)–2(h)] → enlarged bright spots and stripe [Figs. 2(i) and 2(j)] → bright spots at Ce [Fig. 2(k)]. Similarly, the DLFM images transition from the elliptic bright regions at Ce and Co [Figs. 3(a)–3(g)] to the bright regions at M [Figs. 3(h)–3(k)]. In the STM profiles, the first and second inversions of the contrast between Ce and M occur at A_{dith} =2.9 Å and 6.7 Å, respectively [Figs. 4(a) and 4(c)]. In the DLFM images, the inversion occurs at A_{dith}=4.6 Å [Figs. 4(b) and 4(d)]. Thus Figs. 2(j), 3(g), and 3(h) correspond to the patterns near the contrast inversion.

The A_{dith} dependence of Δf_{TR} along P-Q can be explained as follows. First, the lateral force as a function of the dithering coordinate y is simply modeled as $F_{\mathrm{TR}}(y,z) = F_{\mathrm{TR}}^0(z)\sin(2\pi y/L)$, where y=0 and $L/2$ are assumed to correspond to the positions of Ce and M, respectively. Then, Eq. (2) gives,

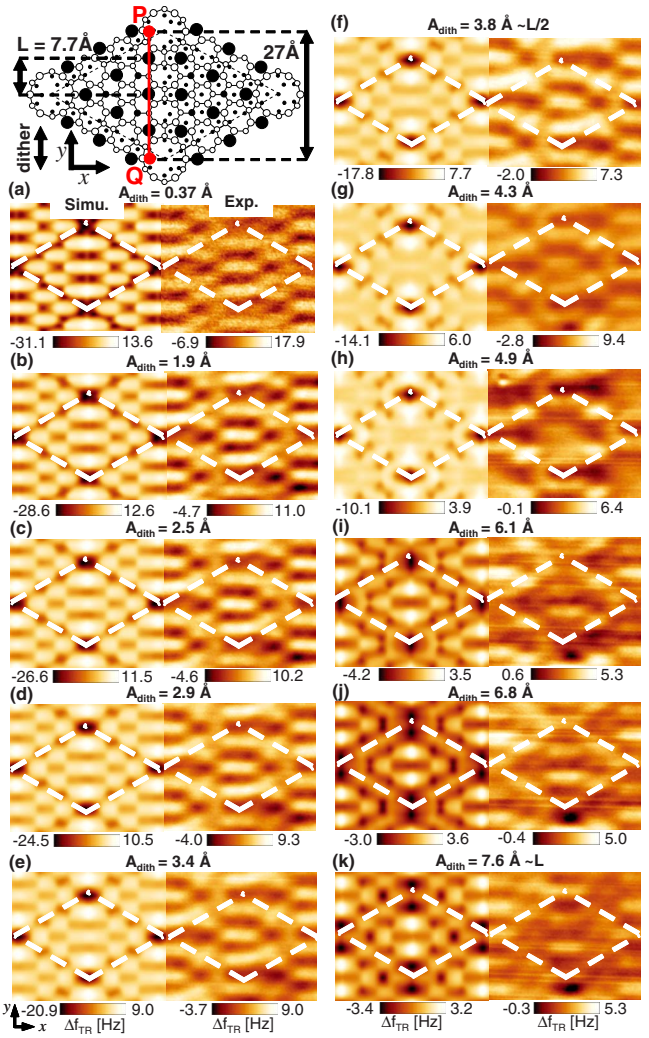

FIG. 3. (Color online) Simulated (left) and experimental (right) DLFM images for A_{dith}= (a) .37, (b) 1.9, (c) 2.5, (d) 2.9, (e) 3.4, (f) 3.8($\simeq L/2$), (g) 4.3, (h) 4.9, (i) 6.1, (j) 6.8, and (k) 7.6($\simeq L$) Å. Imaging parameters: f_{TR}=2.2 MHz, $Q_{\mathrm{TR}}\simeq 1.1\times 10^5$, $\bar{I}_t$=0.5 nA, and V_{bias}=1.8 V. The lateral position of the DLFM images is calibrated by considering the thermal drift.

$$\Delta f_{\mathrm{TR}}[y;z_{\mathrm{STM}}(A_{\mathrm{dith}})] = -\frac{f_{\mathrm{TR}}}{k_{\mathrm{TR}}A_{\mathrm{dith}}}F^0_{\mathrm{TR}}(z_{\mathrm{STM}})\cos\left(\frac{2\pi y}{L}\right)J_1\left(\frac{2\pi A_{\mathrm{dith}}}{L}\right), \quad (3)$$

where J_1 is the first-order Bessel function. Considering $J_1(2\pi A_{\mathrm{dith}}/L)\rightarrow \pi A_{\mathrm{dith}}/L$ for $A_{\mathrm{dith}}\rightarrow 0$, Eq. (3) leads to the well-known formula under the small-amplitude limit, $\Delta f_{\mathrm{TR}} \rightarrow -f_{\mathrm{TR}}\cdot F'_{\mathrm{TR}}/2k_{\mathrm{TR}}$. Next, for the fixed atomic site y, the expression of the normalized reduction rate of $\Delta f_{\mathrm{TR}}(A_{\mathrm{dith}})$ as compared to $\Delta f_{\mathrm{TR}}(A_{\mathrm{dith}}=0)$, $R(A_{\mathrm{dith}})$, is derived as

$$R(A_{\mathrm{dith}}) = \frac{\Delta f_{\mathrm{TR}}(A_{\mathrm{dith}})}{\Delta f_{\mathrm{TR}}(A_{\mathrm{dith}}=0)} = \frac{F^0_{\mathrm{TR}}[z_{\mathrm{STM}}(A_{\mathrm{dith}})]}{F^0_{\mathrm{TR}}[z_{\mathrm{STM}}(A_{\mathrm{dith}}=0)]}\cdot\frac{L}{\pi A_{\mathrm{dith}}}J_1\left(\frac{2\pi A_{\mathrm{dith}}}{L}\right), \quad (4)$$

which is independent of the lateral tip position y. If

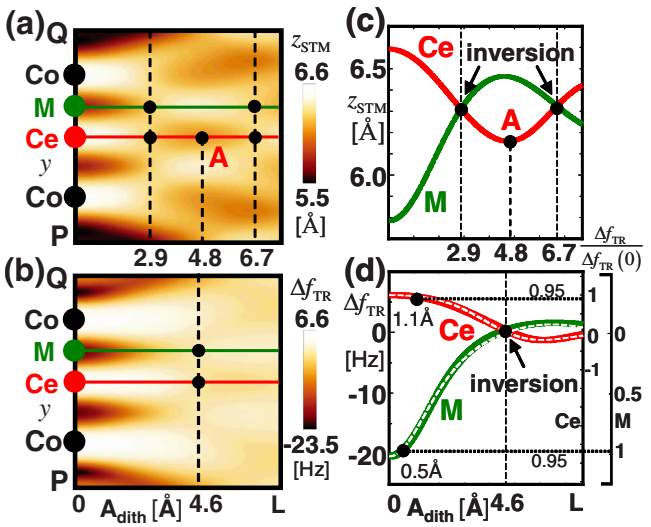

FIG. 4. (Color online) Simulated maps of (a) $z_{\mathrm{STM}}(A_{\mathrm{dith}},y)$ and (b) $\Delta f_{\mathrm{TR}}(A_{\mathrm{dith}},y)$ for $\bar{I}_t$=0.5 nA. (c) and (d) correspond to the cross sections of (a) and (b) at Ce and M. White broken curves in (d) show Eq. (4), $R(A_{\mathrm{dith}})=\Delta f_{\mathrm{TR}}(A_{\mathrm{dith}})/\Delta f_{\mathrm{TR}}(A_{\mathrm{dith}}=0)$ at Ce and M.

$F^0_{\mathrm{TR}}(A_{\mathrm{dith}})/F^0_{\mathrm{TR}}(A_{\mathrm{dith}}=0)$ is evaluated using $F^0_{\mathrm{TR}}(z) \propto e^{-2\kappa(z-z_0)}-e^{-\kappa(z-z_0)}$, with fitting parameters of κ =1.270 Å^{-1} and z_0=2.375 Å obtained by Pérez *et al.*,[22,23] Eq. (4) can excellently explain the simulated results at Ce and M [Fig. 4(d)]. It is easily confirmed that $R(0)=1$. The simulated results indicate that the dithering amplitude at Ce and M must be set as $A_{\mathrm{dith}}\leq 1.1$ and 0.5 Å in order to measure Δf_{TR} within 95% of the theoretical value $\Delta f_{\mathrm{TR}}(A_{\mathrm{dith}}=0)$ [Fig. 4(d)]. This explains the fact that our previous measurement of A_{dith}=0.81 Å falls within a suitable operation range.[13] A similar condition has been pointed out by Sugimoto *et al.*;[6] who reported that A_{dith}=1 Å is sufficiently small to obtain F'_{TR} on the Si(111)-7×7 surface directly by DLFM. Thus, if F'_{TR} is evaluated by the relation $F'_{\mathrm{TR}}=-2k_{\mathrm{TR}}\cdot\Delta f_{\mathrm{TR}}/f_{\mathrm{TR}}$ for finite A_{dith}, the unavoidable underestimation $|F'_{\mathrm{TR}}(A_{\mathrm{dith}})/F'_{\mathrm{TR}}(A_{\mathrm{dith}}=0)|=|R(A_{\mathrm{dith}})|<1$ occurs. However, this feature can be used for the calibration of A_{dith} of STM/DLFM.

It has been previously reported that the relaxation of the tip apex and surface atoms markedly contributes to the atomic resolution.[6,8,9,18,22,24–27] In particular, in the case of the Si(111)7×7 surface, significant vertical and lateral relaxations occur below the critical tip-sample distance of 5 Å. On the other hand, the present simulation shows that the tip-sample distance at Ce and M ranges from 6.2 to 6.6 Å and from 5.8 to 6.5 Å, respectively [Fig. 4(c)]. At Ce, even when the tip comes closest to the surface at z_{STM} =6.2 Å [Fig. 4(c) A], the maximum of $|F_y|$ is only 1.7 pN during one dithering period, $T_{\mathrm{TR}}=1/f_{\mathrm{TR}}$=0.45 μs. The preliminary molecular mechanics simulation of the Si(111) tip comprised of 9454 Si atoms using the Tersoff potential,[28] exhibits the effective lateral spring constant of the tip-apex atom, $k^{\mathrm{atom}}_{\mathrm{TR}}\simeq 6.8$ N/m, which gives the lateral atom displacement $|\Delta y^{\mathrm{atom}}|\simeq 2.5\times 10^{-3}$ Å for $|F_y|\simeq 1.7$ pN. The order of magnitude of the lateral stiffness of the surface adatom is expected to be the same as that of the tip, $k^{\mathrm{atom}}_{\mathrm{TR}}$. Thus, in

the present work, the tip and the surface relaxations are sufficiently small to have negligible influences on the two-dimensional patterns of the STM/DLFM maps. This result shows that STM/DLFM for a small $\bar{I}_t$ can minimize the influence of the tip and surface relaxations. For a larger $\bar{I}_t$ corresponding to $z \leq 5$ Å,[25] the simulation of the STM/DLFM maps considering the atomic relaxation is required.

In this study, we investigated the lateral dithering-amplitude dependence of two-dimensional maps of STM/DLFM on Si(111)7×7 using simulations and experiments. The observed maps are well reproduced and explained by the simulated maps. This work gives the direct calibration of the lateral amplitude of STM/DLFM maps of Si(111)7×7.

One of the authors (N.S.) acknowledges the support by the Grant-in-Aid for Scientific Research (B) from the JSPS (Grant No. 20360022). This work was also supported by MEXT through a Grant-in-Aid for Building Strategic Research Infrastructures. S.K. and H.K. acknowledge the financial support of JST-CREST. Furthermore, N.S. thanks Takahiro Ishikawa for the preliminary evaluation of the tip stiffness.

*naru@st.seikei.ac.jp

[1] C. M. Mate, G. M. McClelland, R. Erlandsson, and S. Chiang, Phys. Rev. Lett. **59**, 1942 (1987).
[2] A. Socoliuc, E. Gnecco, S. Maier, O. Pfeiffer, A. Baratoff, R. Bennewitz, and E. Meyer, Science **313**, 207 (2006).
[3] F. J. Giessibl, Science **267**, 68 (1995).
[4] A. Schwarz, H. Hölscher, S. M. Langkat, and R. Wiesendanger, in *Scanning Tunneling Microscopy/Spectroscopy and Related Techniques*, AIP Conf. Proc. No. 696 (AIP, New York, 2003) p. 68.
[5] M. Ternes, C. P. Lutz, C. F. Hirjibehedin, F. J. Giessibl, and A. J. Heinrich, Science **319**, 1066 (2008).
[6] Y. Sugimoto, T. Namikawa, K. Miki, M. Abe, and S. Morita, Phys. Rev. B **77**, 195424 (2008).
[7] B. J. Albers, T. C. Schwendemann, M. Z. Baykara, N. Pilet, M. Liebmann, E. I. Altman, and U. D. Schwarz, Nat. Nanotechnol. **4**, 307 (2009).
[8] Y. Sugimoto, P. Jelinek, P. Pou, M. Abe, S. Morita, R. Perez, and O. Custance, Phys. Rev. Lett. **98**, 106104 (2007).
[9] Y. Sugimoto, K. Miki, M. Abe, and S. Morita, Phys. Rev. B **78**, 205305 (2008).
[10] O. Pfeiffer, R. Bennewitz, A. Baratoff, E. Meyer, and P. Grutter, Phys. Rev. B **65**, 161403(R) (2002).
[11] F. J. Giessibl, M. Herz, and J. Mannhart, Proc. Natl. Acad. Sci. U.S.A. **99**, 12006 (2002).
[12] S. Kawai, S. Kitamura, D. Kobayashi, and H. Kawakatsu, Appl. Phys. Lett. **87**, 173105 (2005).
[13] S. Kawai, N. Sasaki, and H. Kawakatsu, Phys. Rev. B **79**, 195412 (2009).
[14] N. Sasaki and M. Tsukada, Jpn. J. Appl. Phys. **37**, L533 (1998).
[15] N. Sasaki and M. Tsukada, Jpn. J. Appl. Phys. **38**, 192 (1999).
[16] C. J. Chen, *Introduction to Scanning Tunneling Microscopy*, 2nd ed. (Oxford University, New York, 2008).
[17] K. D. Brommer, M. Needels, B. E. Larson, and J. D. Joannopoulos, Phys. Rev. Lett. **68**, 1355 (1992).
[18] R. Pérez, M. C. Payne, I. Stich, and K. Terakura, Phys. Rev. Lett. **78**, 678 (1997).
[19] S. Kawai, D. Kobayashi, S. Kitamura, S. Meguro, and H. Kawakatsu, Rev. Sci. Instrum. **76**, 083703 (2005).
[20] T. R. Albrecht, P. Grutter, D. Horne, and D. Rugar, J. Appl. Phys. **69**, 668 (1991).
[21] F. J. Giessibl, Rev. Mod. Phys. **75**, 949 (2003).
[22] R. Pérez, I. Stich, M. C. Payne, and K. Terakura, Phys. Rev. B **58**, 10835 (1998).
[23] Using fitting parameters shown in Table I in Ref. 22, $\kappa = 2b/R_c = 1.270$ Å^{-1} and $z_0 = R_c = 2.357$ Å are obtained for adatom.
[24] M. A. Lantz, H. J. Hug, R. Hoffmann, P. J. A. van Schendel, P. Kappenberger, S. Martin, A. Baratoff, and H.-J. Guntherodt, Science **291**, 2580 (2001).
[25] D. Sawada, Y. Sugimoto, K. Morita, M. Abe, and S. Morita, Appl. Phys. Lett. **94**, 173117 (2009).
[26] W. A. Hofer, A. S. Foster, and A. L. Shluger, Rev. Mod. Phys. **75**, 1287 (2003).
[27] R. Hoffmann, A. Baratoff, H. J. Hug, H. R. Hidber, H. v. Löhneysen, and H.-J. Güntherodt, Nanotechnology **18**, 395503 (2007).
[28] J. Tersoff, Phys. Rev. Lett. **61**, 2879 (1988).